

MECHANICAL CHARACTERISATION AND
MODELLING OF A THERMOREVERSIBLE
SUPERAMOLECULAR POLYURETHANE OVER A
WIDE RANGE OF RATES

H. Chen^{1*}, L. R. Hart², W. Hayes², C.R. Siviour¹

¹Solid Mechanics and Materials Engineering Department of Engineering Science

University of Oxford, Oxford, United Kingdom, OX1 3PJ

²Department of Chemistry

University of Reading, Reading, United Kingdom, RG6 6DX

*huanming.chen@eng.ox.ac.uk

Supplementary Information

Contents

1 Specimen Preparation.....	2
2 Full DSC Data.....	3
3 Rheometry Data and Modelling.....	7
3.1 Reproducibility.....	7
3.2 Model by shift method.....	7
3.3 Arrhenius equation-based model.....	13
3.4 Modelling high temperature relaxation.....	16
4 Viscoelasticity and Prony Series Modelling.....	18
5 Viscoelastic Softening Model.....	23
6 Specimen Geometries for Recovery Analysis.....	24
7 Full Experimental Data for Low-to-high Strain Rates.....	26
8 Model outputs.....	28

1 Specimen Preparation

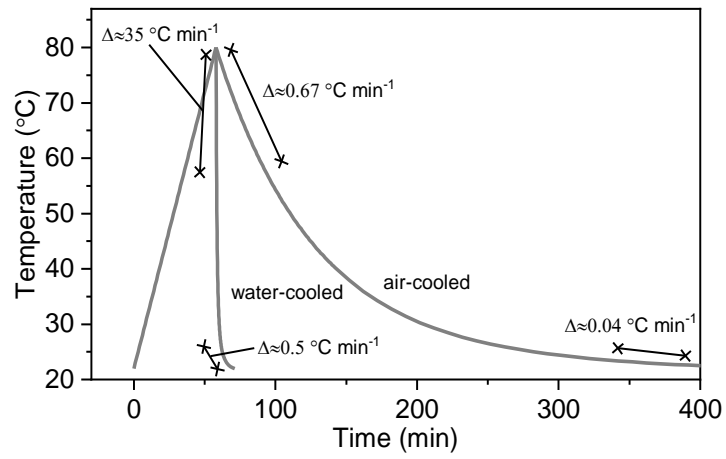


Figure SI 1: Temperature profiles for air- and water-cooled specimens

2 Full DSC Data

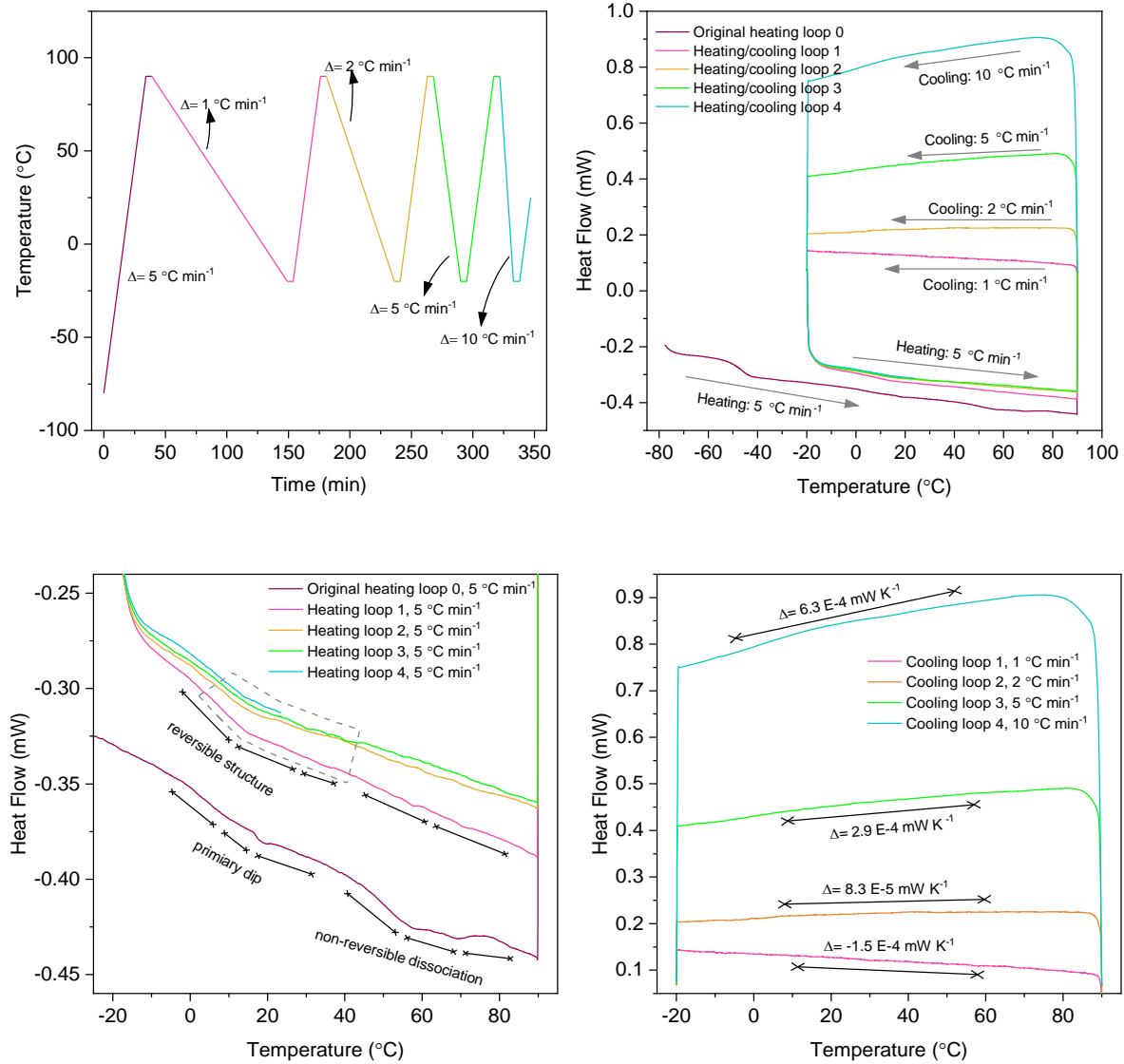


Figure SI 2: DSC experiments for 'Sample DSC1' with different cooling rates performed on a cast (raw) specimen: (a) temperature profile used; (b) measured heat flow for the different heating and cooling loops; (c) detail of heating loops; (d) detail of cooling loops.

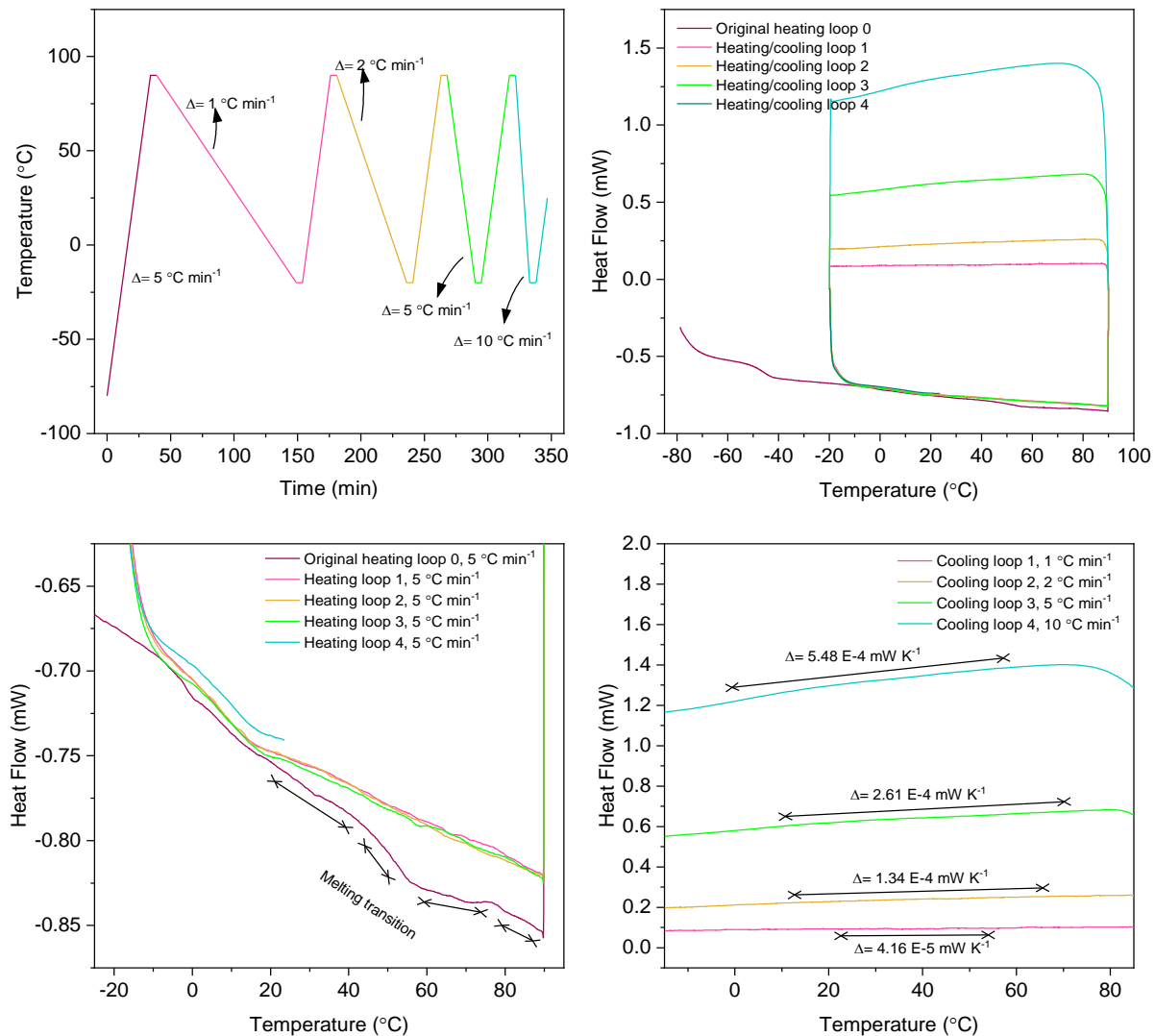


Figure SI 3: DSC experiments for 'Sample DSC2' with different cooling rates performed on a cast (raw) specimen: (a) temperature profile used; (b) measured heat flow for the different heating and cooling loops; (c) detail of heating loops; (d) detail of cooling loops.

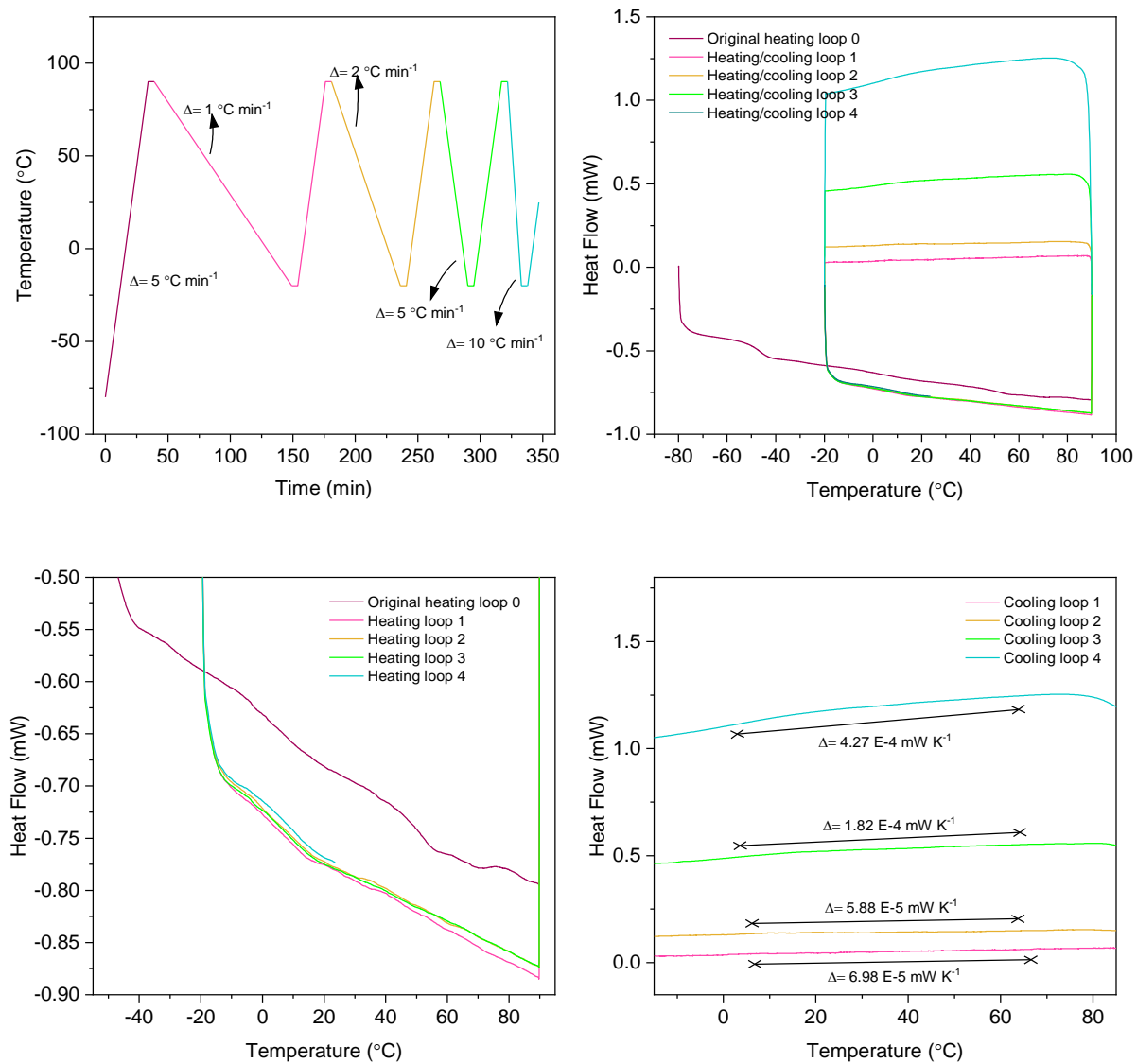


Figure SI 4: DSC experiments for 'Sample DSC3' with different cooling rates performed on an cast (raw) specimen: (a) temperature profile used; (b) measured heat flow for the different heating and cooling loops; (c) detail of heating loops; (d) detail of cooling loops.

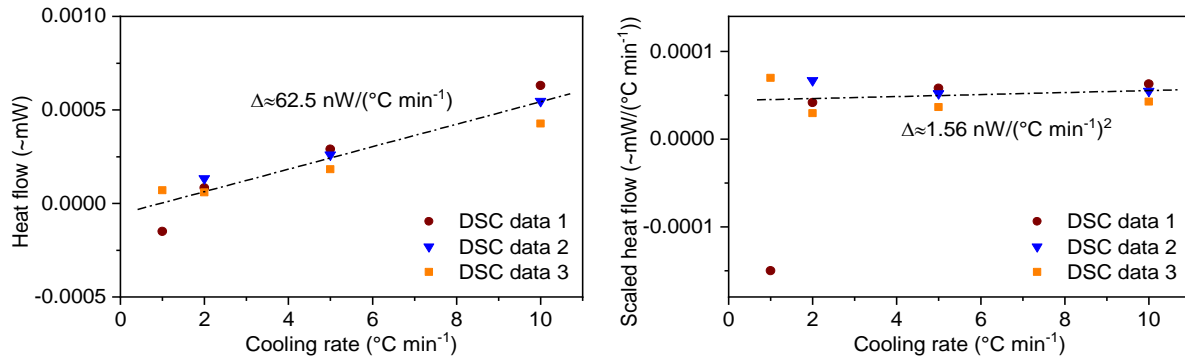


Figure SI 5: (a) Heat flow against cooling rate in each DSC loop; (b) Heat flow normalized by the cooling rate to give a scaled unit value, which is almost consistent for each rate, indicating that the underlying thermodynamic process is not affected by cooling rate.

3 Rheometry Data and Modelling

3.1 Reproducibility

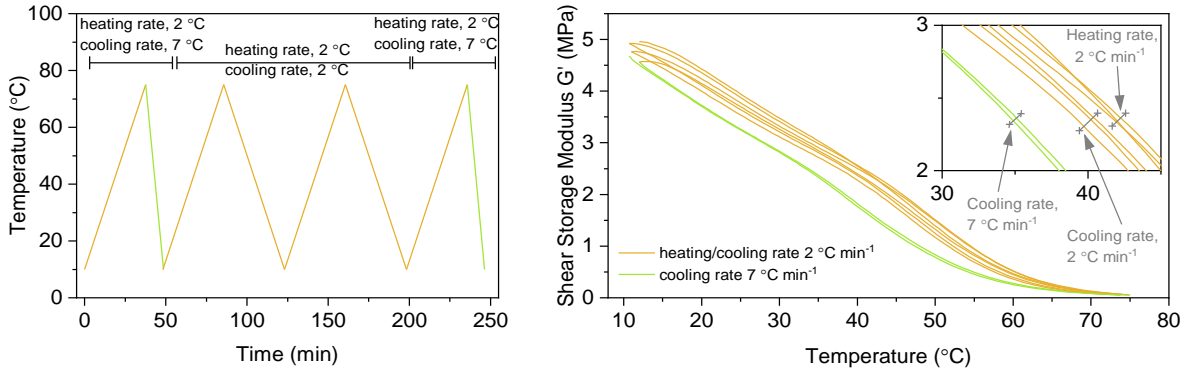


Figure SI 6: The reproducibility of the rheological data was confirmed by conducting repeated dynamic rheological analysis at two rates, to see whether the temperature history was fully erased in each new thermal cycle. A single specimen was heated at 2 °C min⁻¹ and cooled at 7 °C min⁻¹, followed by 2 °C min⁻¹ twice, and then 7 °C min⁻¹ again.

3.2 Model by shift method

In the ‘shift method’, the modulus-temperature curves produced by different heating or cooling rates in main paper are shifted horizontally to overlap at a ‘reference’ rate, here 2 °C min⁻¹. The shifted curves are shown in *Figure SI 7* along with the required shift factors, which were modelled using an equation, similar to the formation of the WLF equation (introduced in *Section 4*), given by

$$SF = -\frac{\alpha(\dot{T} - \dot{T}_{ref})}{\beta + (\dot{T} - \dot{T}_{ref})} \quad Eq. (1)$$

where α and β are fitting parameters, \dot{T} is the cooling or heating rate and, \dot{T}_{ref} is the reference rate. The parameters were obtained by fitting to the empirical data, after which it was observed that the parameters fit the same relation in both heating and cooling experiments.

This relationship was then validated, again using a reference curve at 2 °C min⁻¹, at cooling rates of 3, 8, 12 °C min⁻¹, *Figure SI 8*. These experiments were performed at temperatures from 0

to 90 °C; a comparison of these data to the earlier rheometry results, *Figure SI 9*, shows good agreement. Here the limitations of the Peltier temperature control system in the rheometer should be noted; in particular, that the cooling rate decreases towards the end of each cooling ramp. This causes discrepancies in the data around room temperature in the first set of experiments and around 0 °C in the second set. Details of the temperature-time profiles are shown in *Figures SI 10 and 11*.

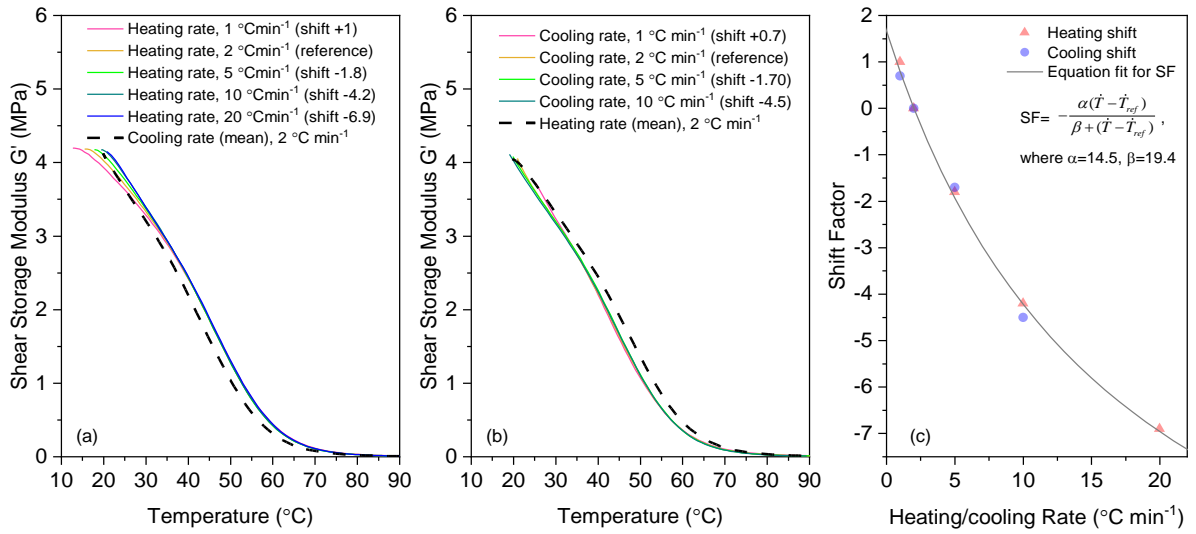


Figure SI 7: (a) and (b) The modulus-temperature curves obtained at different temperatures can be horizontally shifted to overlap; this produces a rate dependent shift factor shown in (c). Oscillation frequency 1 Hz and amplitude 0.1%.

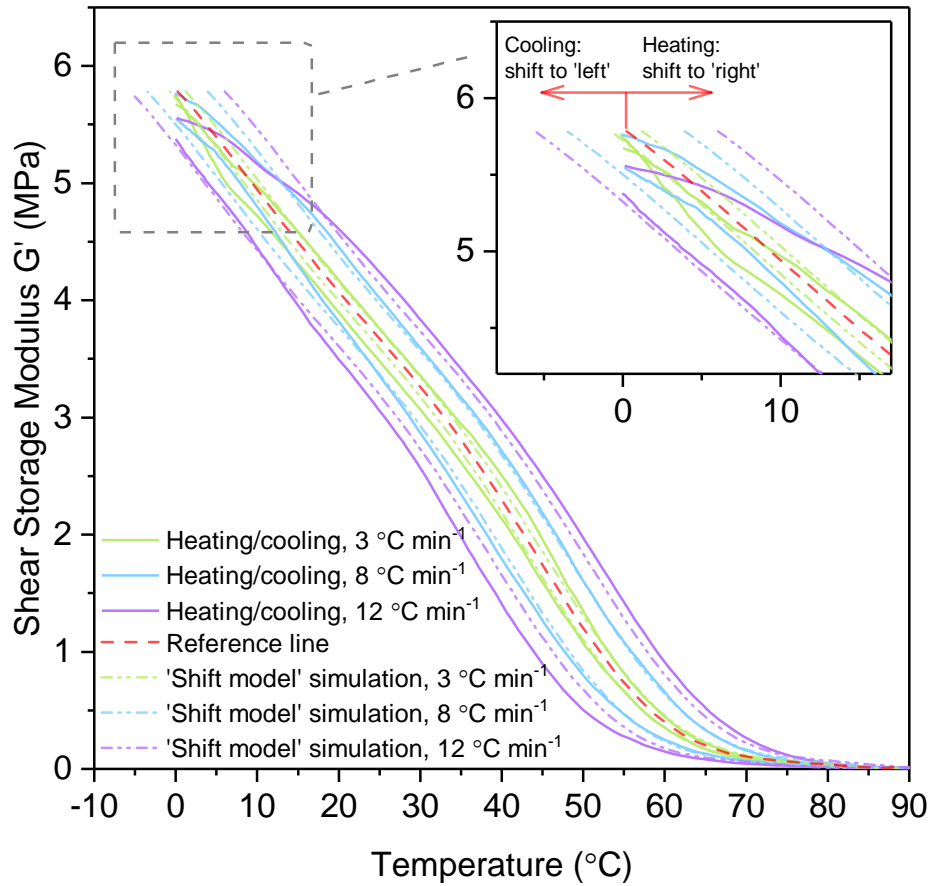
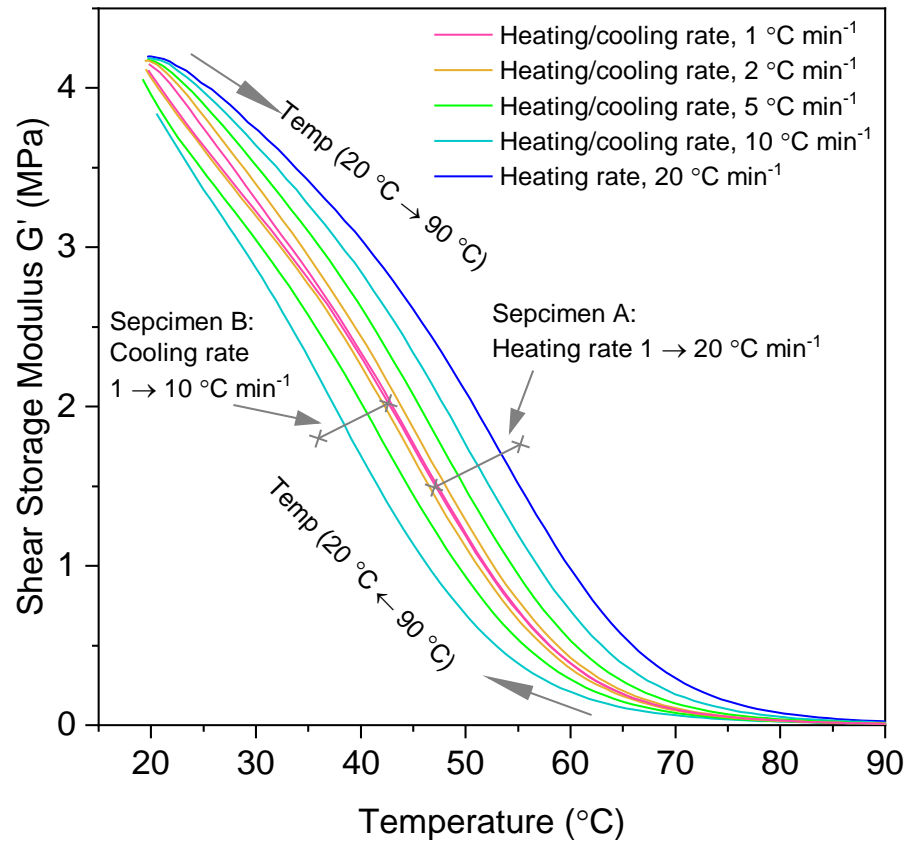


Figure SI 8: Application of the 'shift method' using previously obtained shift factors to describe the rheological data at 3, 8, 12 $^{\circ}\text{C min}^{-1}$. The reference curve was extrapolated from the average of the data obtained at 2 $^{\circ}\text{C min}^{-1}$. Oscillation frequency 1 Hz and amplitude 0.1%.



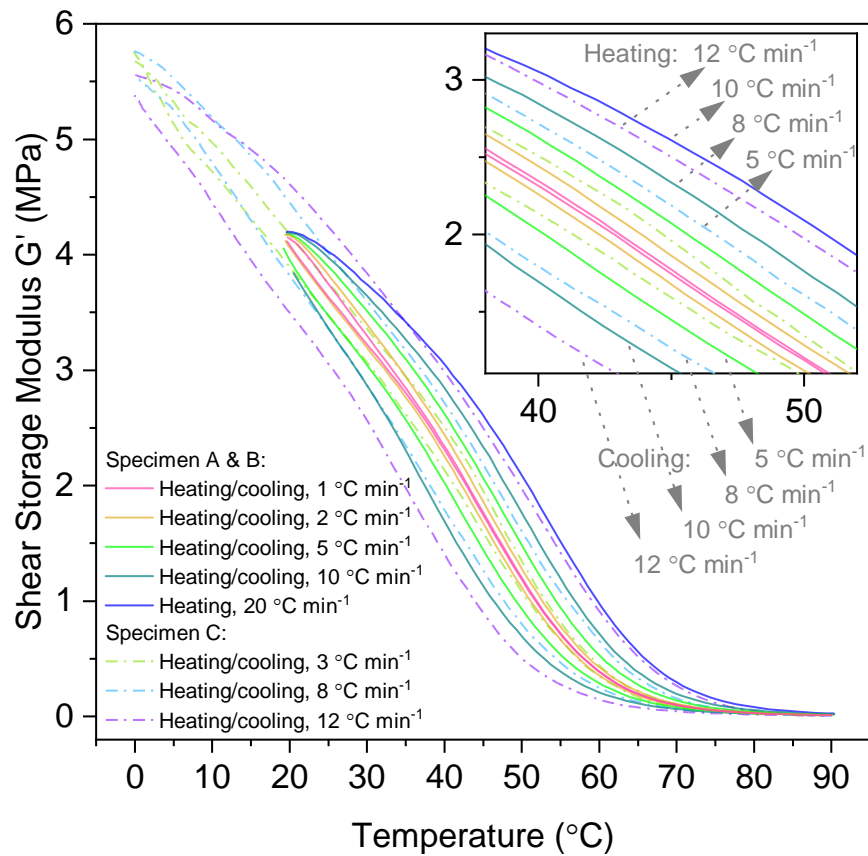


Figure SI 9: Comparison of rheological data from three different samples: (a) assembled data from specimens A & B which underwent heating/cooling rates of 1, 2, 5, 10, 20 $^{\circ}\text{C min}^{-1}$, also shown in the main text, Figure 7. (b) comparison of the combination of data A & B to the specimen C, the latter was tested at rates of 3, 8, 12 $^{\circ}\text{C min}^{-1}$ over a wider temperature range. Oscillation frequency 1 Hz and amplitude 0.1%.

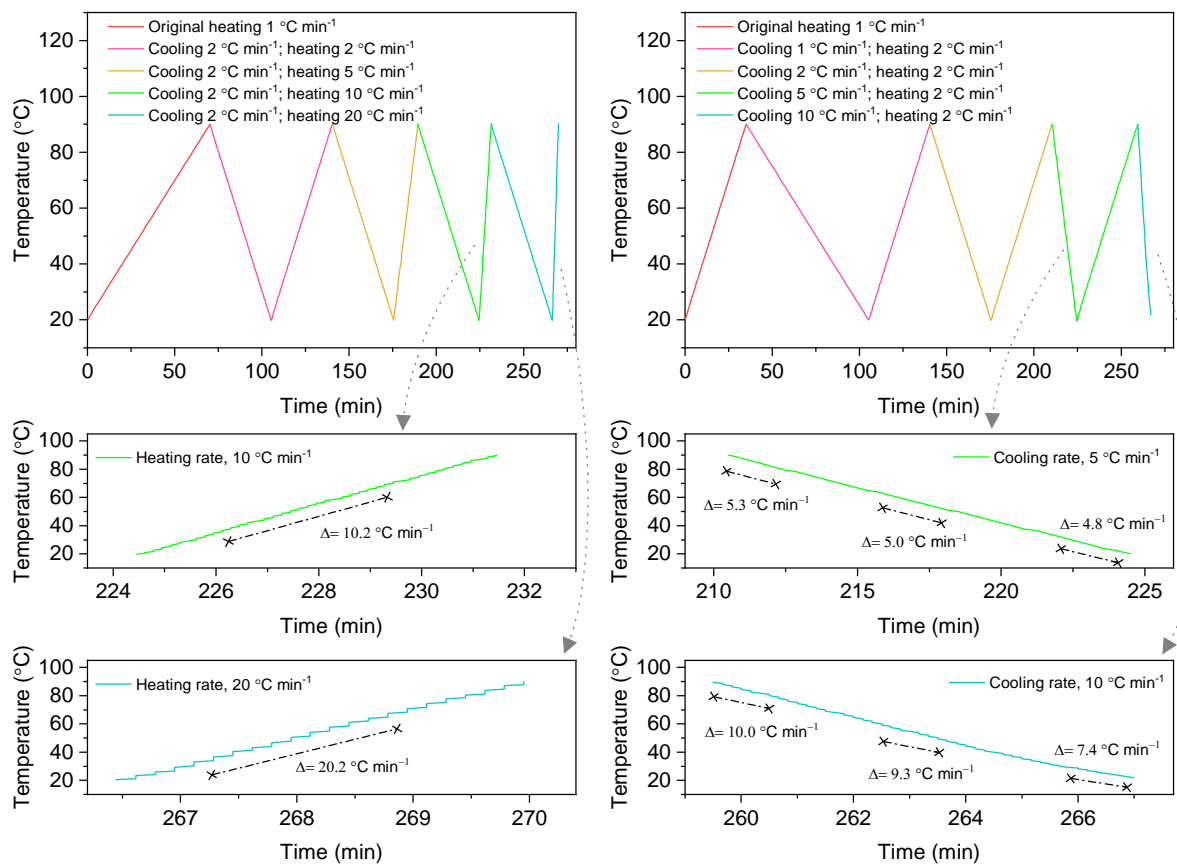


Figure SI 10: The temperature profile for rheological analysis at heating and cooling rates of 1, 2, 5, 10 and 20 °C min⁻¹. The Peltier temperature control system has good consistency in slow cooling and fast heating, but for fast cooling the rate decreased towards the end of the cycle.

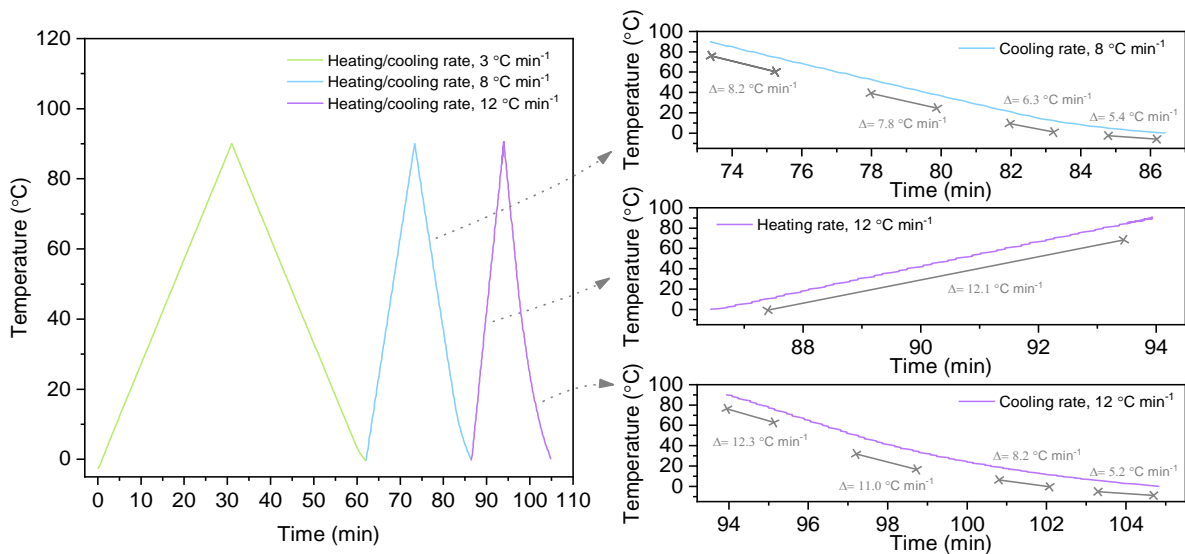


Figure SI 11: The temperature profile for rheological analysis at heating and cooling rates of 3, 8 and 12 °C min⁻¹.

3.3 Arrhenius equation-based model

The parameters derived in the main text ($r_0 = 2 \text{ s}^{-1}$ and $U/k = 1312 \text{ K}$) were used to model the experiments with nominal temperature profiles of 3, 8, 12 °C min⁻¹ (*Figure SI 11*), results are shown in *Figure SI 12*. The advantage of this model over the shifting method is that, in principle, it can be applied to arbitrary temperature profiles, and the parameters have a better physical interpretation, as rate of evolution and thermal activation. It was also noted that this model has better continuity than the ‘shift method’ for thermal cycles because it can use the experimental temperature profiles. To demonstrate the importance this, model outputs at different constant heating/cooling rates are shown in *Figure SI 13* whilst a comparison of results from constant and empirical rates is shown in *Figure SI 14*.

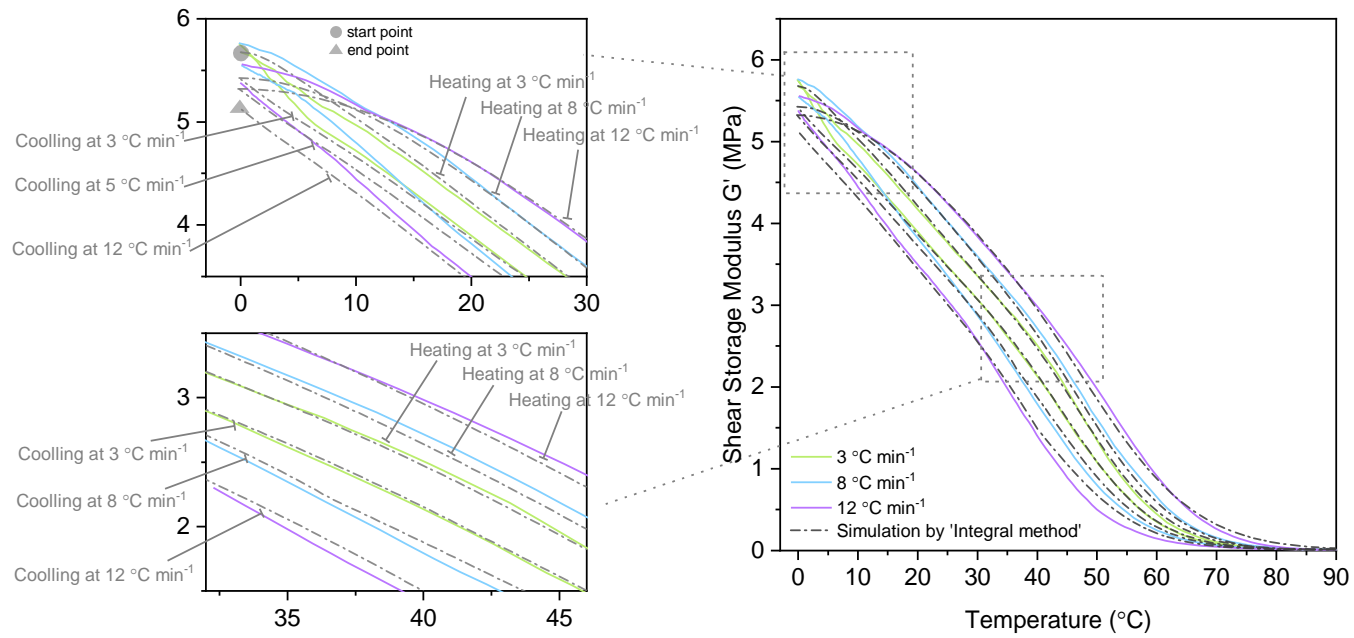


Figure SI 12: Application of the Arrhenius equation based model to heating and cooling processes at 3, 8, 12 $^{\circ}\text{C min}^{-1}$. The reference curve was produced by extrapolation of the previous reference curve. The same parameters as in Figure 11 and the experimental temperature profiles were applied. Oscillation frequency 1 Hz and amplitude 0.1%.

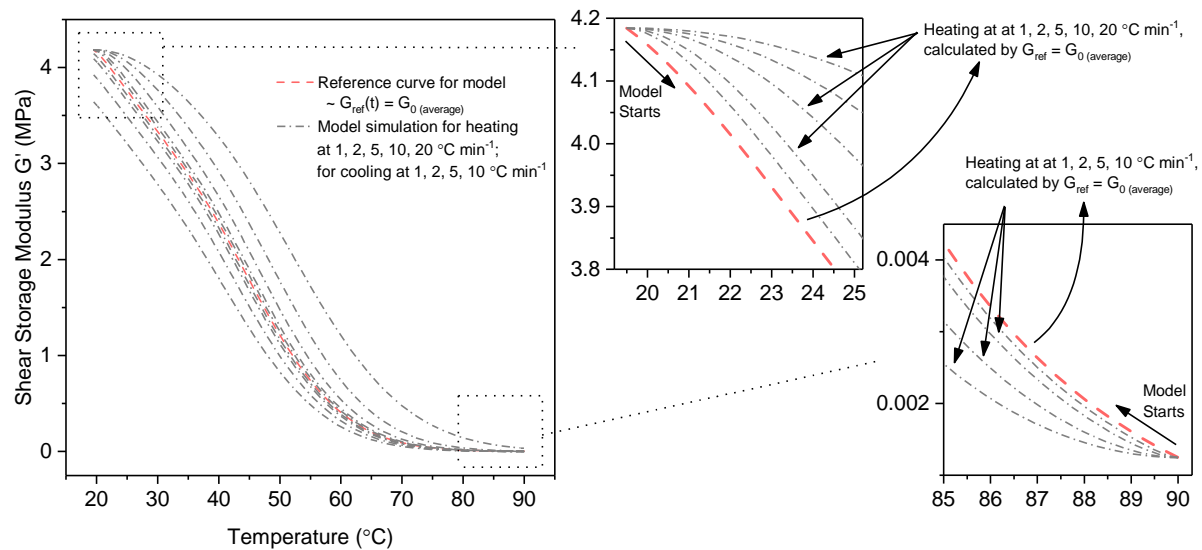


Figure SI 13: An example of applying the Arrhenius equation based model to heating/cooling processes from 1 to 20 °C min⁻¹. Here, a constant heating or cooling rate is assumed. Oscillation frequency 1 Hz and amplitude 0.1%.

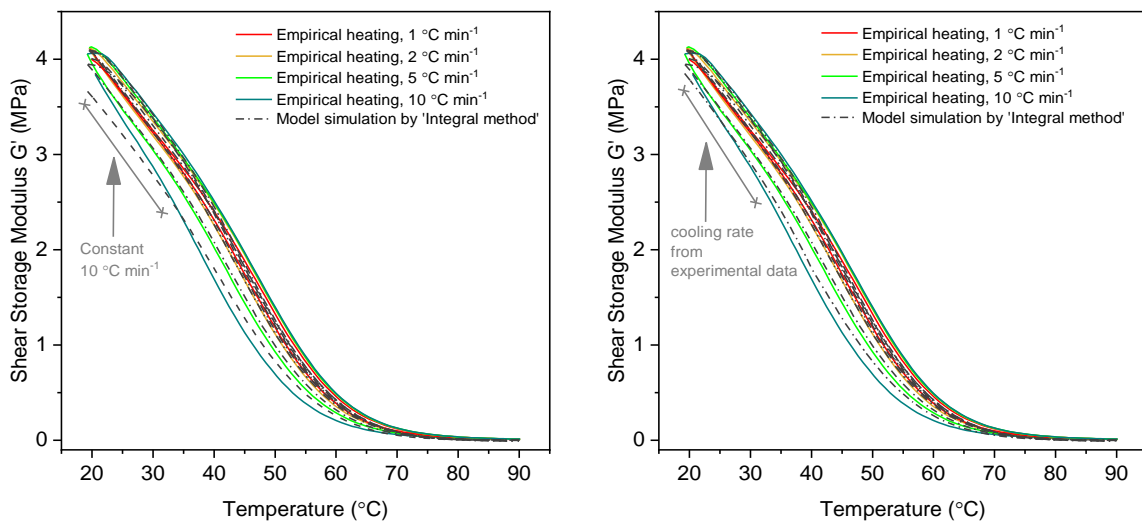


Figure SI 14: Comparison of data obtained using (a) constant cooling rate of 10 °C and (b) the empirical cooling rate, in Arrhenius equation based model. Oscillation frequency 1 Hz and amplitude 0.1%.

3.4 Modelling high temperature relaxation

A final rheological experiment was performed to investigate the evolution of mechanical response when held at 80 °C; here all the heating and cooling cycles were performed at 2 °C min⁻¹, whilst during the hold the specimen was maintained at a strain of 0.1 % with no oscillation. The data obtained are shown in *Figure SI 15*. Here, *Figure SI 15a*, shows the temperature profiles used whilst *Figure SI 15b* shows that the storage modulus profiles are consistent between cycles. Finally, *Figure SI 15c* shows the relaxation of the modulus with time at 80 °C. In particular, it is interesting to re-derive the Arrhenius parameters to fit these data. An estimate of the long-term modulus was taken as the reference, G_{ref} , whilst r_0 and U/k were fit to the relaxation data: the resulting value of r_0 was the same as obtained from the previous fit, whilst U/k was different. In order to confirm that these differences are significant, a comparison of model outputs for heating and cooling cycles using three values of U/k is shown in *Figure SI 16*. The changes in value indicate that there may be more than one process involved in the polymer response, with different activation energies.

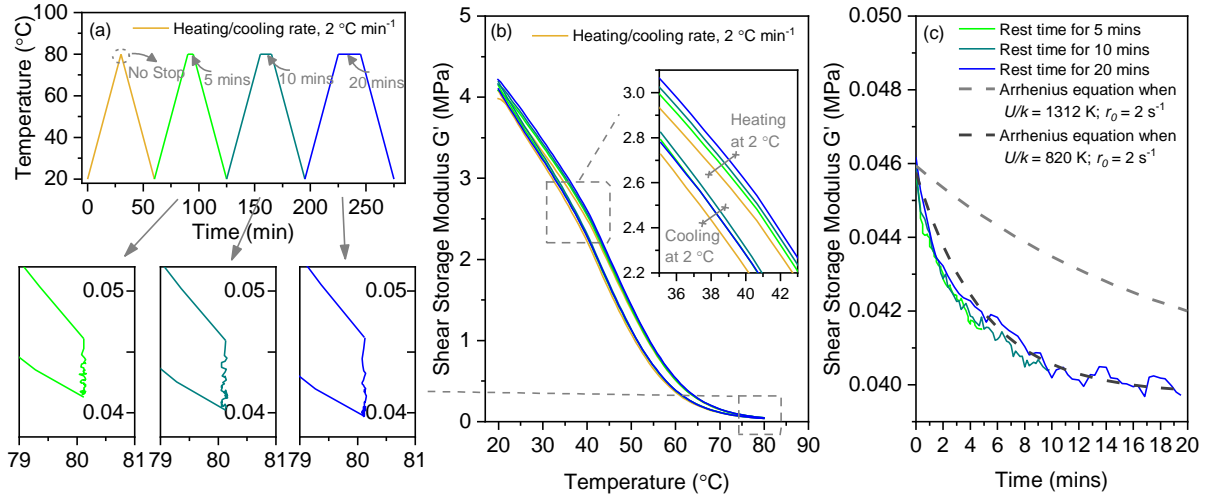


Figure SI 15: One single specimen subjected to rheological analysis at $2\text{ }^{\circ}\text{C min}^{-1}$ on both heating and cooling but held for different times between 0 and 20 minutes at $80\text{ }^{\circ}\text{C}$. (a) heating profiles (b) The mechanical behavior during heating and cooling is consistent, also shown is a magnification of the detail at $80\text{ }^{\circ}\text{C}$. (c) The Arrhenius equation based model was applied again to model the high temperature relaxation. Here, G_{ref} was set equal to 0.0397 MPa , estimated from the long-term stress response from the experiments. Unit r_0 is s^{-1} , U/k is K . Changing the activation energy term U/k from 1312 K to 820 K gives a better fit to the experimental data.

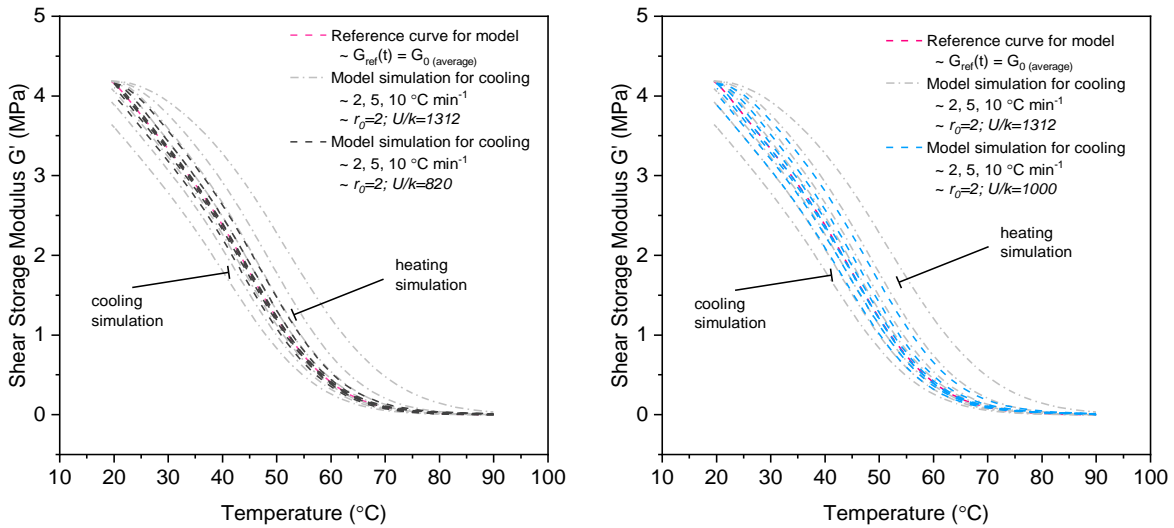


Figure SI 16: Comparisons of the Arrhenius based Integral model using three different values of U/k : 1312 , 820 and 1000 K for heating and cooling simulation.

4 Viscoelasticity and Prony Series Modelling

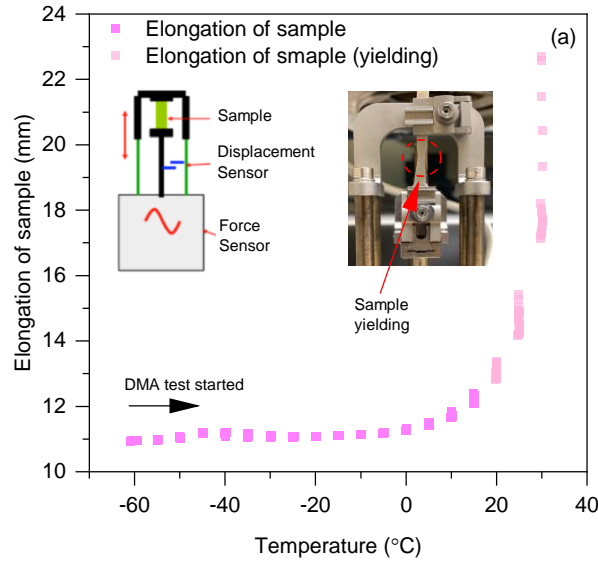


Figure SI 17: Specimen elongation and necking were observed in DMA experiments at temperatures over 15 °C.

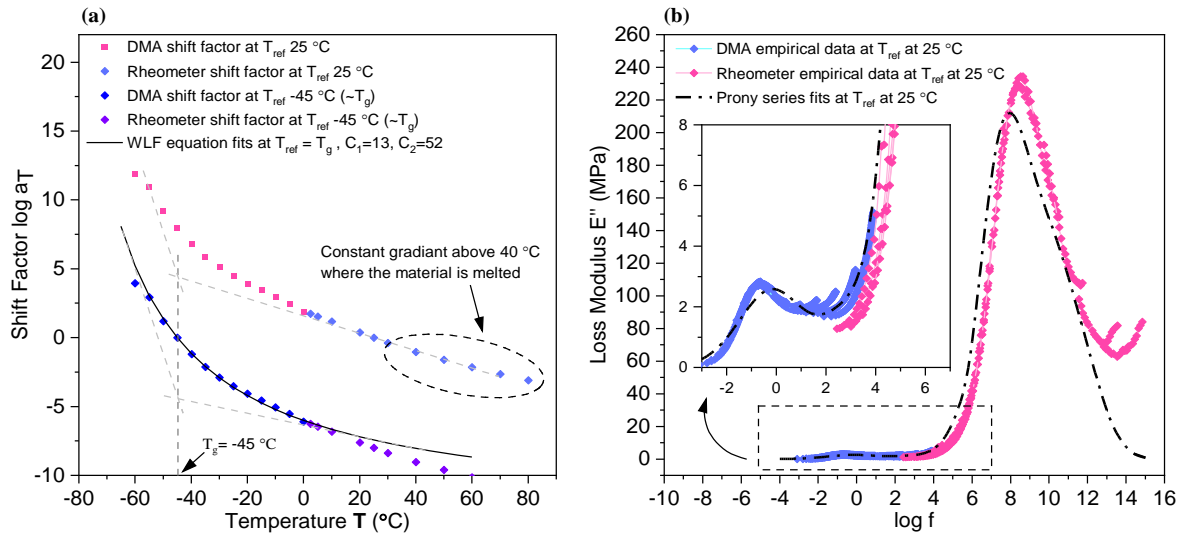


Figure SI 18: (a) Plot of shift factor vs temperature for master curves produced at 25 and -45 °C. The WLF equation with parameters $C_1=13$, $C_2=52$ °C fits the shift factors. (b) The Prony series fit to the storage data can be used to derive loss modulus as a function of frequency; here it is compared to empirical data.

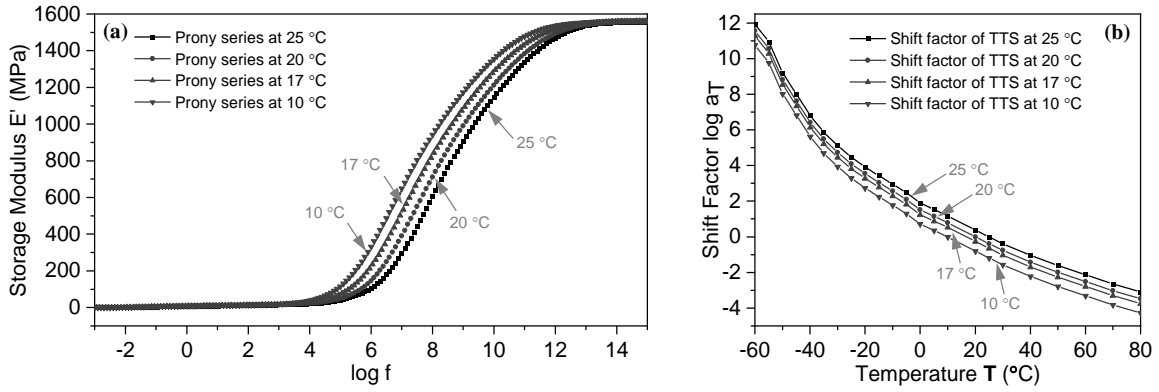


Figure SI 19: The Prony series and TTS shift factors for reference temperatures of 25, 20, 17 and 10 °C.

Table SI 1: Prony Series at 25 °C

Maxwell Element Number	Young's Moduli <i>E</i> (MPa)	Relaxation Time τ (s)	Viscosity η (Pa · s)
N/A	0.000	$+\infty$	$+\infty$
1	0.268	1.778E+02	4.769E+01
2	0.741	5.623E+01	4.164E+01
3	1.758	1.778E+01	3.126E+01
4	2.340	5.623E+00	1.315E+01
5	2.097	1.778E+00	3.728E+00
6	1.587	5.623E-01	8.923E-01
7	1.378	1.778E-01	2.449E-01
8	1.420	5.623E-02	7.986E-02
9	1.420	1.778E-02	2.524E-02
10	1.344	5.623E-03	7.557E-03
11	1.334	1.778E-03	2.371E-03
12	1.515	5.623E-04	8.519E-04
13	2.469	1.778E-04	4.390E-04
14	5.710	5.623E-05	3.210E-04
15	12.667	1.778E-05	2.252E-04
16	22.184	5.623E-06	1.247E-04
17	33.113	1.778E-06	5.888E-05
18	70.830	5.623E-07	3.983E-05
19	117.73	1.778E-07	2.093E-05
20	154.84	5.623E-08	8.707E-06
21	169.45	1.778E-08	3.013E-06
22	162.30	5.623E-09	9.126E-07
23	144.05	1.778E-09	2.561E-07
24	125.96	5.623E-10	7.083E-08
25	112.75	1.778E-10	2.005E-08
26	102.31	5.623E-11	5.753E-09
27	90.52	1.778E-11	1.609E-09
28	75.64	5.623E-12	4.253E-10
29	58.88	1.778E-12	1.047E-10
30	42.09	5.623E-13	2.366E-11
31	26.27	1.778E-13	4.671E-12
32	12.86	5.623E-14	7.236E-13
33	5.506	1.778E-14	9.791E-14

Table SI 2: Prony Series at 20 °C

Maxwell Element Number	Young's Moduli <i>E</i> (MPa)	Relaxation Time τ (s)	Viscosity η (Pa · s)
N/A	0.000	$+\infty$	$+\infty$
1	0.838	1.778E+02	1.490E+02
2	1.842	5.623E+01	1.035E+02
3	2.316	1.778E+01	4.118E+01
4	2.072	5.623E+00	1.165E+01
5	1.594	1.778E+00	2.834E+00
6	1.362	5.623E-01	7.659E-01
7	1.389	1.778E-01	2.470E-01
8	1.396	5.623E-02	7.847E-02
9	1.269	1.778E-02	2.256E-02
10	1.220	5.623E-03	6.859E-03
11	1.520	1.778E-03	2.703E-03
12	2.325	5.623E-04	1.307E-03
13	4.102	1.778E-04	7.294E-04
14	8.469	5.623E-05	4.762E-04
15	18.406	1.778E-05	3.273E-04
16	36.848	5.623E-06	2.072E-04
17	73.496	1.778E-06	1.307E-04
18	120.34	5.623E-07	6.767E-05
19	156.36	1.778E-07	2.780E-05
20	169.53	5.623E-08	9.533E-06
21	161.37	1.778E-08	2.869E-06
22	142.88	5.623E-09	8.034E-07
23	125.04	1.778E-09	2.223E-07
24	112.11	5.623E-10	6.304E-08
25	101.70	1.778E-10	1.808E-08
26	89.74	5.623E-11	5.046E-09
27	74.69	1.778E-11	1.328E-09
28	57.87	5.623E-12	3.254E-10
29	41.11	1.778E-12	7.311E-11
30	25.38	5.623E-13	1.427E-11
31	12.21	1.778E-13	2.172E-12
32	5.35	5.623E-14	3.012E-13
33	8.99	1.778E-14	1.599E-13

Table SI 3: Prony Series at 17 °C

Maxwell Element Number	Young's Moduli E (MPa)	Relaxation Time τ (s)	Viscosity η (Pa · s)
N/A	0.000	$+\infty$	$+\infty$
1	1.352	1.778E+02	2.404E+02
2	2.171	5.623E+01	1.220E+02
3	2.257	1.778E+01	4.013E+01
4	1.821	5.623E+00	1.024E+01
5	1.435	1.778E+00	2.552E+00
6	1.363	5.623E-01	7.662E-01
7	1.416	1.778E-01	2.518E-01
8	1.349	5.623E-02	7.587E-02
9	1.224	1.778E-02	2.175E-02
10	1.324	5.623E-03	7.445E-03
11	1.855	1.778E-03	3.298E-03
12	3.032	5.623E-04	1.705E-03
13	5.805	1.778E-04	1.032E-03
14	12.53	5.623E-05	7.048E-04
15	26.46	1.778E-05	4.706E-04
16	52.05	5.623E-06	2.927E-04
17	97.12	1.778E-06	1.727E-04
18	140.76	5.623E-07	7.916E-05
19	166.04	1.778E-07	2.952E-05
20	167.57	5.623E-08	9.423E-06
21	152.64	1.778E-08	2.714E-06
22	133.43	5.623E-09	7.503E-07
23	118.00	1.778E-09	2.098E-07
24	106.86	5.623E-10	6.009E-08
25	96.090	1.778E-10	1.708E-08
26	82.563	5.623E-11	4.642E-09
27	66.384	1.778E-11	1.180E-09
28	49.423	5.623E-12	2.779E-10
29	33.067	1.778E-12	5.880E-11
30	18.293	5.623E-13	1.028E-11
31	7.680	1.778E-13	1.365E-12
32	5.722	5.623E-14	3.217E-13
33	5.113	1.778E-14	8.891E-14

5 Viscoelastic Softening Model

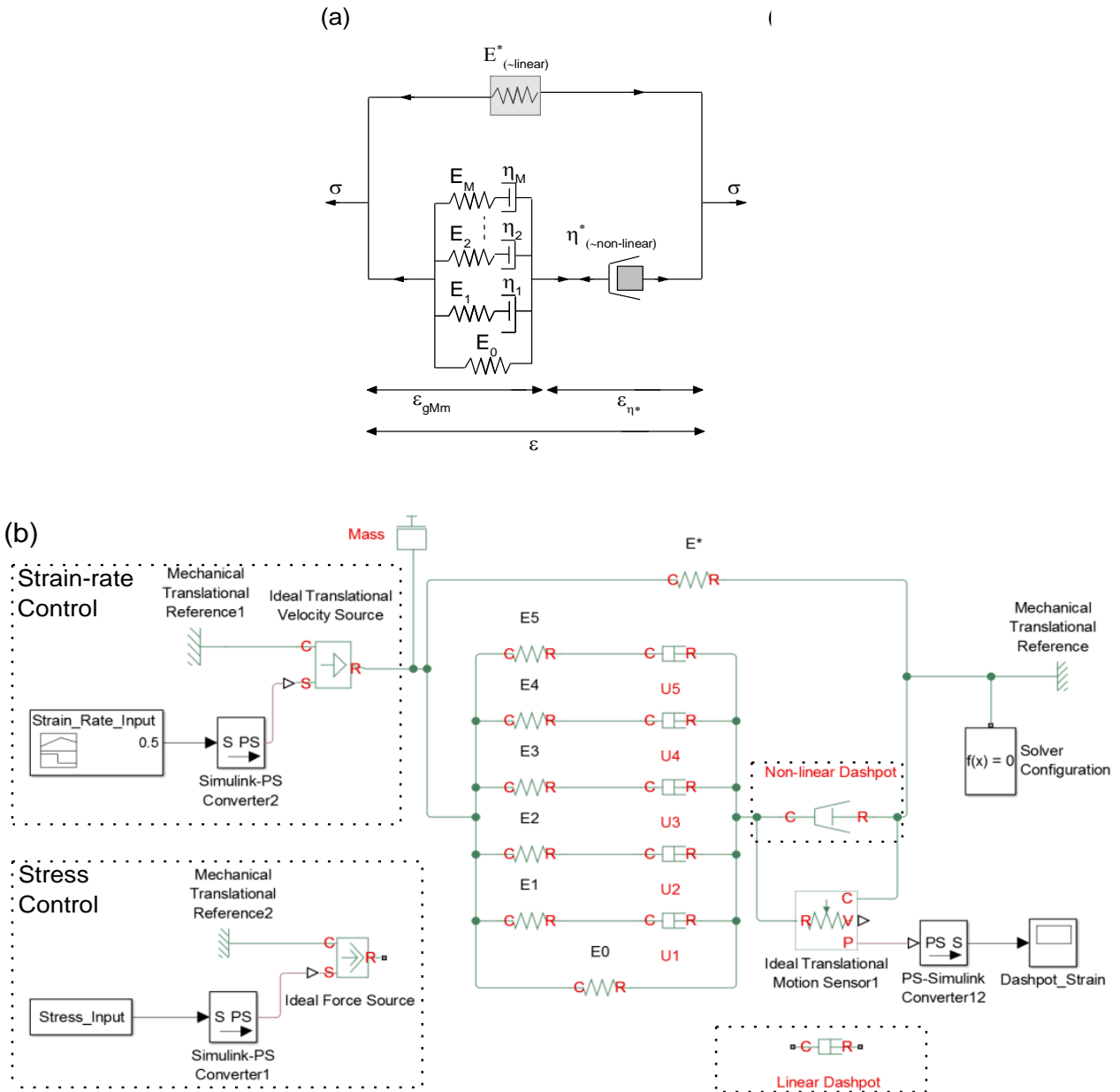


Figure SI 20: The viscoelastic softening model implemented in Simscape and used to describe the mechanical responses including loading, unloading and recovery. (a) The model combines springs and dashpots described by the Prony series, an additional dashpot η^* and a recovery spring E^* . (b) The model implemented in Simulink, the deformation was applied by either a velocity source control or a force control, allowing either strain or stress profiles. A motion sensor measures the strain behaviour in each element but can be replaced by force sensor if stress values are required.

6 Specimen Geometries for Recovery Analysis

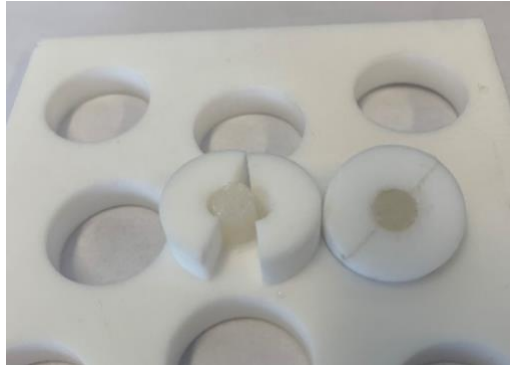


Figure SI 21: Specimen preparation and can be compressed as a cylinder or disk with desired dimension for experiments by using PTFE mould.

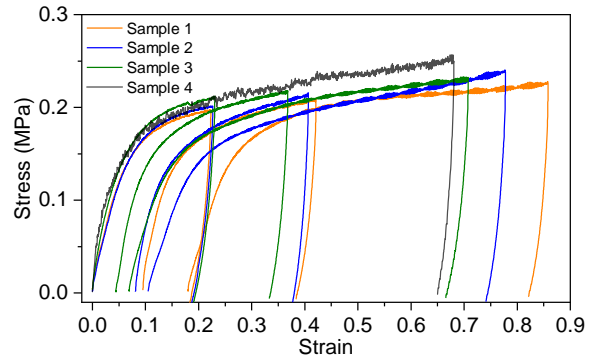


Figure SI 22: Empirical strain-stress curves for three samples for recovery tests: key strain values are given in Table SI4.

Table SI 4: Strain data for Figure SI 22

ε	After Loading	After 3hrs Recover	After 6hrs Recover	After 12hrs Recover
Sample 1				
1st Loading	0.185	0.112	0.09	N/A
$\varepsilon_0/\varepsilon_f$ (%)	100	60.15	48.65	N/A
2nd Loading	0.386	0.248	0.181	N/A
$\varepsilon_0/\varepsilon_f$ (%)	100	64.25	46.89	N/A
Sample 2				
1st Loading	0.190	0.118	0.081	N/A
$\varepsilon_0/\varepsilon_f$ (%)	100	62.25	42.63	N/A
2nd Loading	0.38	N/A	0.145	0.105
$\varepsilon_0/\varepsilon_f$ (%)	100	N/A	38.16	27.63
Sample 3				
1st Loading	0.194	N/A	N/A	0.044
$\varepsilon_0/\varepsilon_f$ (%)	100	N/A	N/A	22.68
2nd Loading	0.335	N/A	N/A	0.0688
$\varepsilon_0/\varepsilon_f$ (%)	100	N/A	N/A	20.54

7 Full Experimental Data for Low-to-high Strain Rates

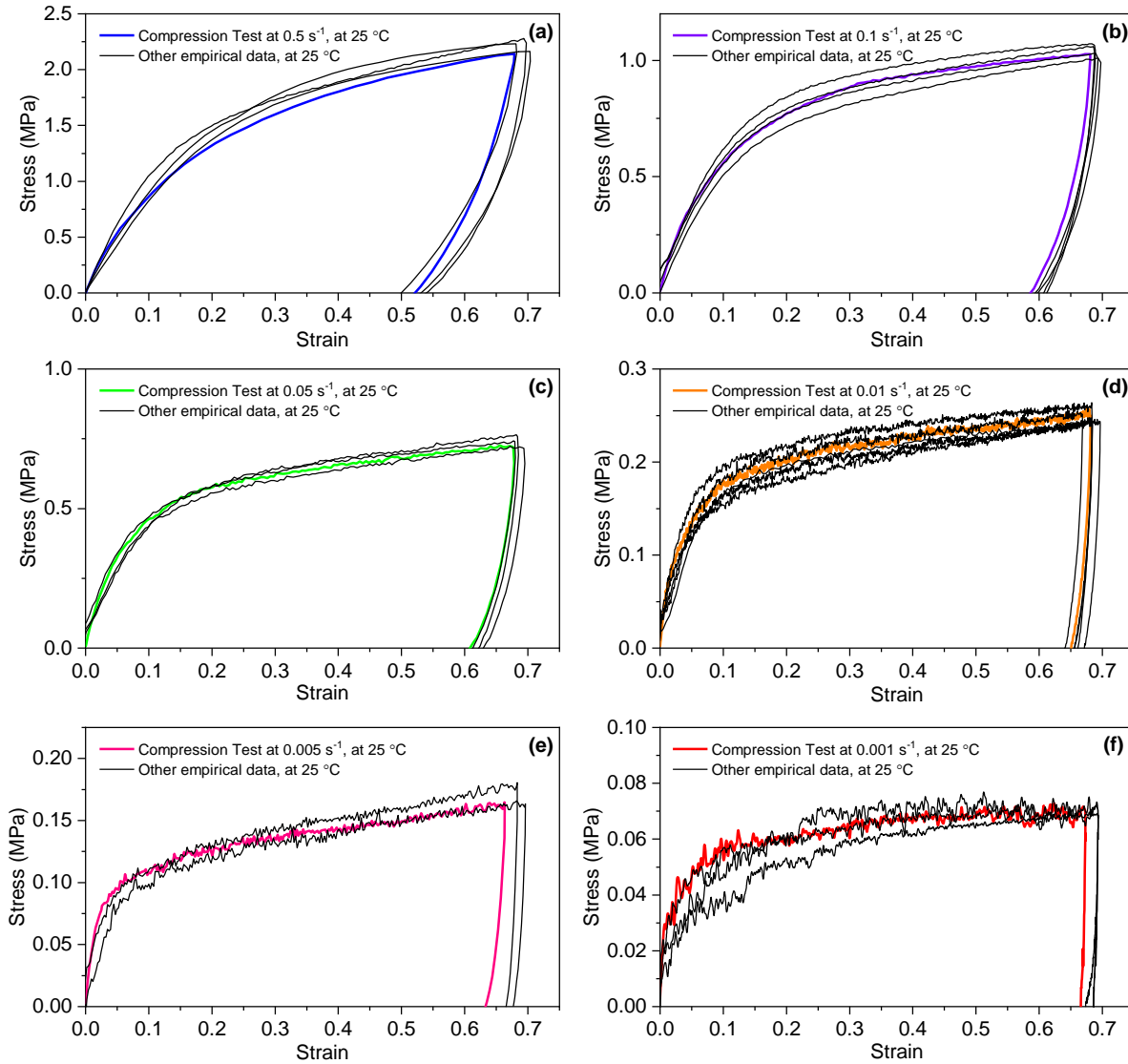


Figure SI 23: Full data of low-rate compression experiments at 25 °C but varying strain rates: 0.001, 0.005, 0.01, 0.05, 0.1, 0.5 s^{-1} . The result used in the main paper is indicated by a coloured line, the other results are presented with black lines.

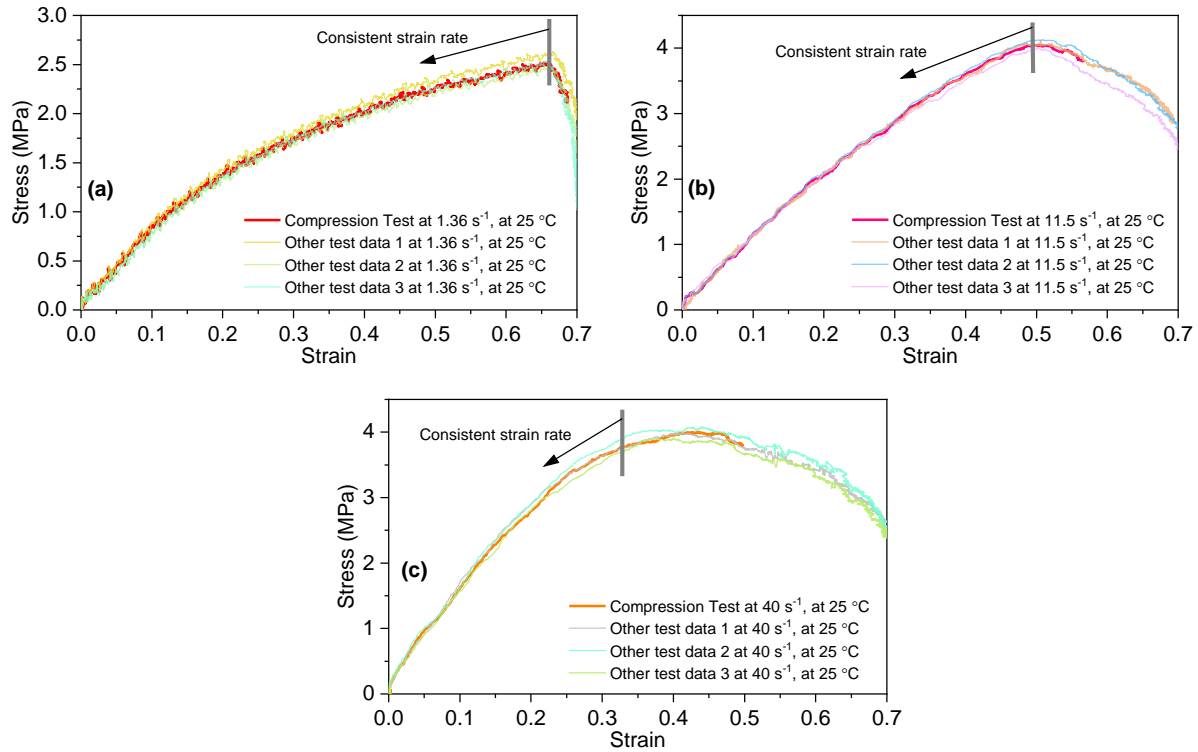


Figure SI 24: Full data of medium-rate compression experiments at 25 °C but varying strain rates: 1.36, 11.5, 40 s⁻¹; regions of constant strain rate are indicated, as are the test data used in the main paper.

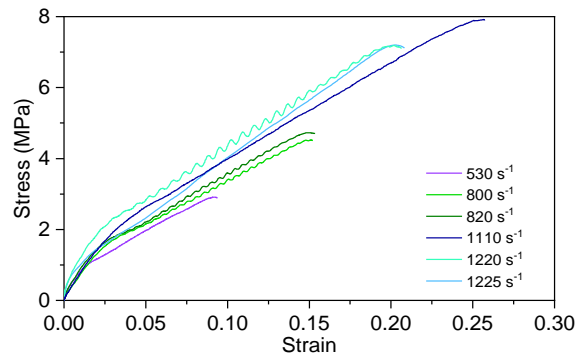


Figure SI 25: Full data from high-rate compression experiments at 17 °C but varying strain rates.

8 Model outputs

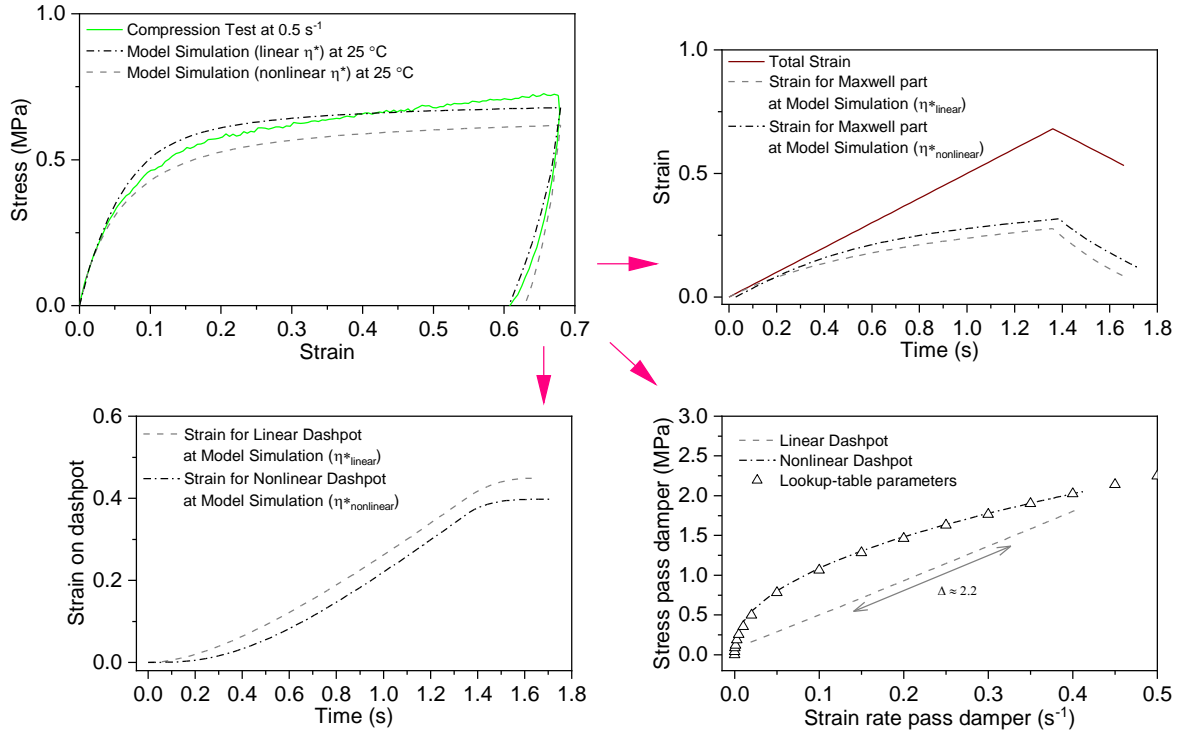


Figure SI 26: The strain history for each element of the model at a strain rate 0.5 s^{-1} at $25 \text{ }^\circ\text{C}$ and the stress and strain rate in the damper.

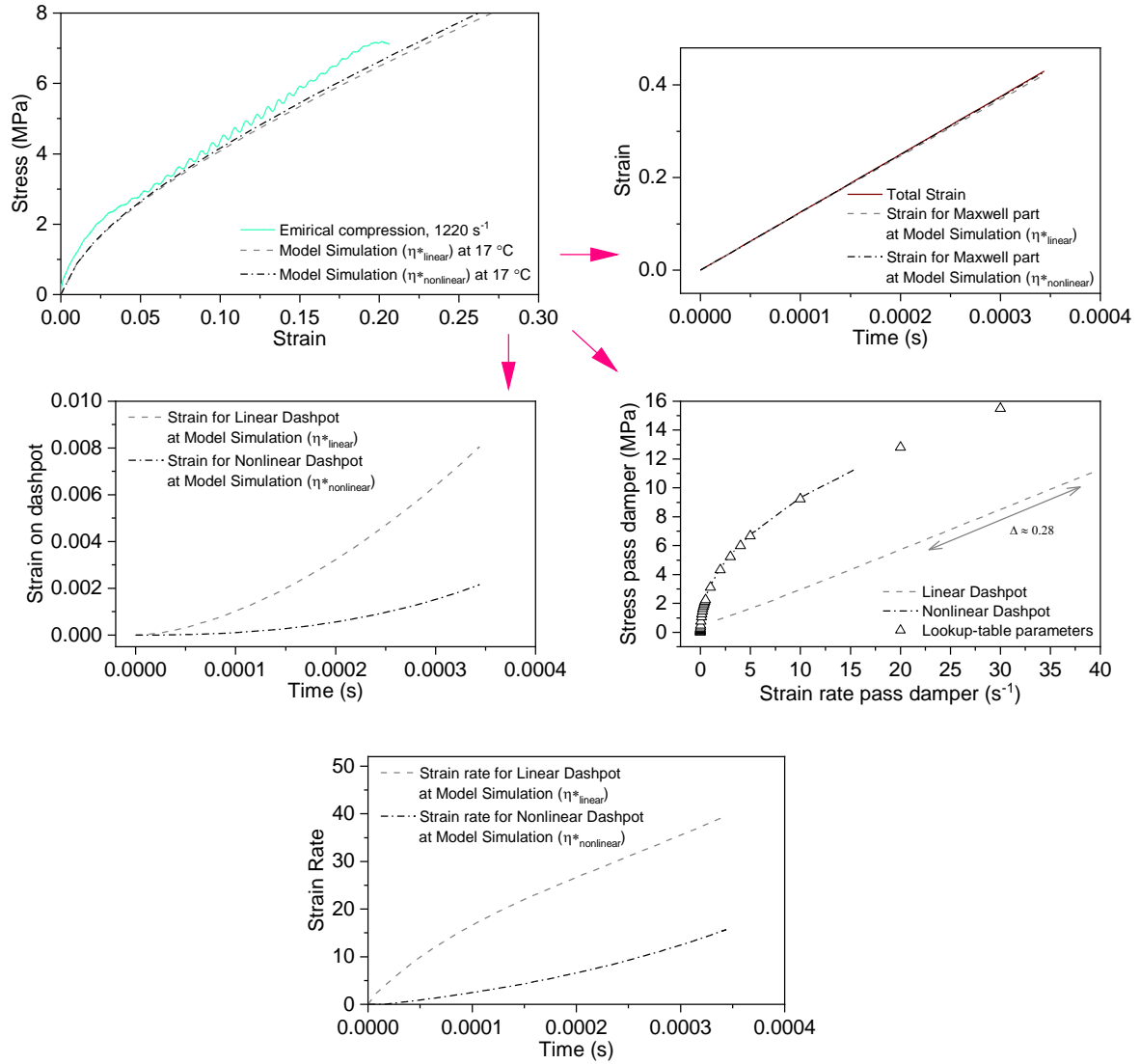


Figure SI 27: The strain history for each element from the model at a strain rate 1220 s^{-1} at $17 \text{ }^{\circ}\text{C}$ and the stress and strain rate in dashpot η^* .

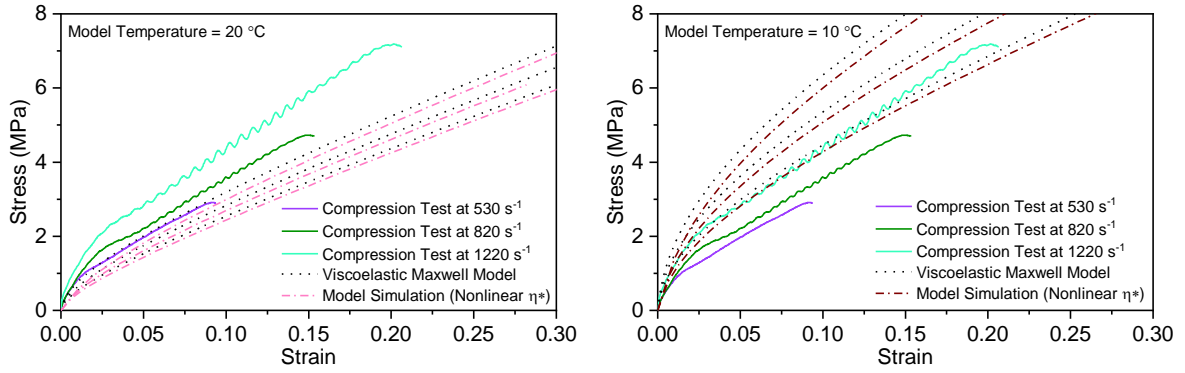


Figure SI 28: Comparison of data obtained using the Prony series to predict the viscoelastic response at high strain rates at 20 and 10 °C. Note the strong temperature sensitivity.

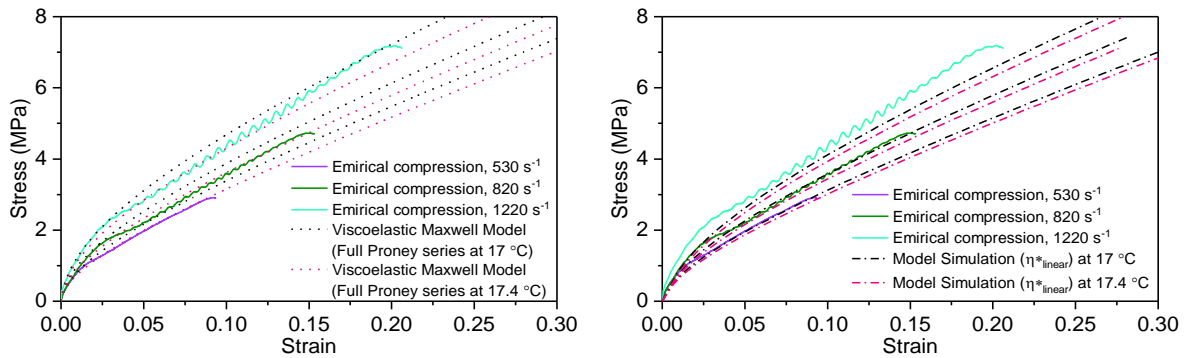


Figure SI 29: Comparison of model outputs using Prony series calibrated at 17 and 17.4 °C, indicating the effect that adiabatic heating could have on the response.